Carbonates Evaporites (2017) 32:261–277
DOI 10.1007/s13146-016-0318-1

ORIGINAL ARTICLE

Early Triassic stromatolites from the Xingyi area, Guizhou Province, southwest China: geobiological features and environmental implications

Shilei Liu[1] · Jian Wang[1,2] · Fuguang Yin[2] · Tao Xie[2] · Shixue Hu[2] · Xiaofeng Guan[1] · Qiyue Zhang[2] · Changyong Zhou[2] · Wanhua Cheng[2] · Jinsha Xu[2]

Accepted: 11 July 2016 / Published online: 9 August 2016

Abstract An Early Triassic stromatolitic deposit is documented in the Dienerian succession of the Lower Triassic Feixianguan Formation in the Xingyi area, Guizhou, southwest China. Five types of constructional microbial forms at various scales were observed. (1) Typical stratified columnar structures, up to 25 cm in height, with crinkled laminae. Dark-coloured laminae, 1 mm thick, are composed of upright filamentous tubes, average diameter 5 μm, showing a vertical growth fabric. (2) Prostrate filaments showing strong fluorescence, in sharp contrast to the micritic cement. (3) Coccoid-like spheroids and algal filaments are also common in stromatolitic laminae. These resemble present-day cyanobacteria, and thus may represent fossilized cyanobacteria. (4) Smaller bacilli resembling *Pelodictyon* are very common in the stromatolitic laminae. (5) Framboidal pyrite is also abundant and probably indicates biological involvement in stromatolite formation. Two major microbial functional groups, oxygenic phototrophs represented by lithified cyanobacteria and probable sulfate-reducing bacteria represented by framboidal pyrite, were present during stromatolite growth. Another possible microbial functional group, anoxygenic phototrophs represented by lithified remains resembling *Pelodictyon clathratiforme*, may be present in the Xingyi stromatolites, and were involved in stromatolite formation by capturing or adhering microcrystalline particles. All of these features demonstrate that the Early Triassic stromatolites are biogenic. The occurrence of the Xingyi stromatolites, corresponding to a second episode of microbial growth during the Early Triassic, reveals that post-extinction microbialites were widespread in the Dienerian. These Early Triassic stromatolites indicate that a microbial bloom took place in the aftermath of the Permian–Triassic mass extinction.

Keywords Early Triassic · Stromatolites · Geobiology · Environmental implications

Introduction

Stromatolites, which possess laminated structures (Riding 2000), are one of the most intriguing benthic microbial deposits. They provide a unique window to investigate the history of photosynthesis, evolution of the early atmosphere and microbe–environment interactions through geological time (Awramik 1992, 2006; Kah and Riding 2007; Kershaw et al. 2007, 2009, 2012; Noffke and Awramik 2013). Early Triassic stromatolites have been reported from around the world (Schubert and Bottjer 1992; Sano and Nakashima 1997; Richoz et al. 2005; Hips and Haas 2006; Pruss et al. 2006; Farabegoli et al. 2007; Kershaw et al. 2011; Chen et al. 2012, 2014; Mata and Bottjer 2012) and are major components of post-extinction microbialites. Resurgence of microbial communities occurred throughout the entire Early Triassic recovery interval, during that time there were at least four major events of high microbialite abundance (Baud et al. 2007). Although three of these stromatolite events have been documented in detail. But there are few examples of Early Triassic stromatolites from the second event. In this study, a stromatolitic deposit from the second event is described. The deposit provides important evidence on the extent of

✉ Jian Wang
w1962jian@163.com

[1] Chengdu University of Technology, Chengdu 610059, China

[2] Chengdu Center of China Geological Servey, Chengdu 610081, China

devastated oceanographic conditions that prevailed in the global ocean during the Early Triassic (Bottjer et al. 2008; Chen et al. 2010; Algeo et al. 2011; Chen and Benton 2012).

Microbialites deposits (stromatolites, thrombolites and other forms) formation is often interpreted as the outcome of combined reduction in metazoan diversity and rising seawater saturation state in respect to $CaCO_3$ (Riding and Liang 2005; Kershaw et al. 2007, 2012; Woods et al. 2007). However, recent studies show that the biogenic mechanisms were involved in microbialite formation. Microbes play an important role in accretion, lamination and early lithification of modern marine stromatolites forming in open marine environments of normal seawater salinity as on the margins of Exuma Sound, Bahamas (Reid et al. 2000). During periods of rapid sedimentation, filamentous cyanobacteria dominate over the stromatolite surfaces, whereas the climax communities of endolithic coccoidal bacteria develop during prolonged hiatal periods (Reid et al. 2000). This viewpoint opens a brand new window insight into the possible forming mechanism of microbialite deposits (Ezaki et al. 2003, 2008; Hips and Haas 2006; Kershaw et al. 2011, 2012; Yang et al. 2011; Chen et al. 2014; Luo et al. 2014).

The aims of this study are: (1) to describe the microbial structure and composition of the Xingyi stromatolites; (2) to elucidate the accretion and formation processes of the stromatolites; and (3) to discuss the possible palaeoenvironmental implications.

Geological background

The stromatolites described in this study were collected from the Bayou Section of the Xingyi area, about 12 km southwest of Xingyi city, southwestern Guizhou Province, southwest China (Fig. 1). The Xingyi area is situated in the northwestern part of the Nanpanjiang Basin, which is located on the eastern part of the Khandian platform. The Xingyi area is separated from the Nanpanjiang Basin by a shoal complex (Feng et al. 1994). In the Bayou Section, upper Permian mudstone and skeletal limestones are unconformably overlain by the Feixianguan Formation, which are in turn overlain by the Jialingjiang Formation.

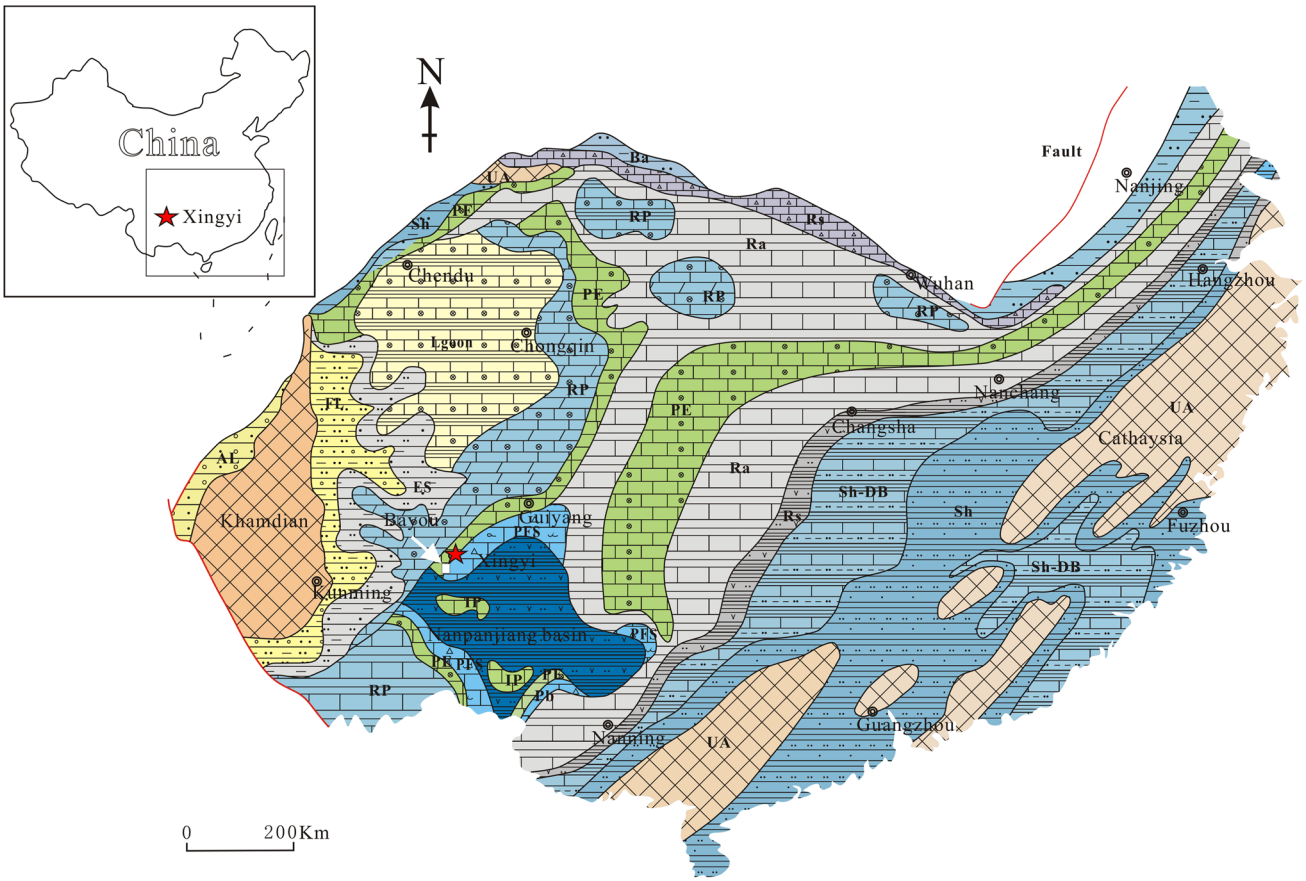

Fig. 1 Early Triassic palaeogeographic map of south China showing the palaeogeographic setting of the Xingyi area (*red pentagon*) during that time [base map was modified from Feng et al. (1994)]

The Feixianguan Formation is subdivided into two Members. Member I is dominated by pewter-coloured siliciclastic sediments, representing deposition in a subtidal to intertidal environment. Laminated clastic deposits were widely developed during the earliest part of the Early Triassic, immediately after the Permian–Triassic boundary mass extinction in the upper Yangtze area, representing sluggish oceanic circulation.

From field observations and logged sections, Member II of the Feixianguan Formation consists of two units (Fig. 2). Unit 1 (23.4–103 m) contains thick bedded siltstone and fine sandstone. The siltstone is partly fossiliferous— mainly bivalve fossils. The original physical sedimentary structures of the rock are tidal bedding and cross-bedding. The fine grained sediments represent intertidal to subtidal facies. Unit 1 in the lower part of Member II is similar to Member I, and consists mainly of siltstone and sandstone deposited in an intertidal to subtidal settings. Unit 2 (103–369.2 m) is composed of thin-bedded muddy limestone and alternations of oolitic

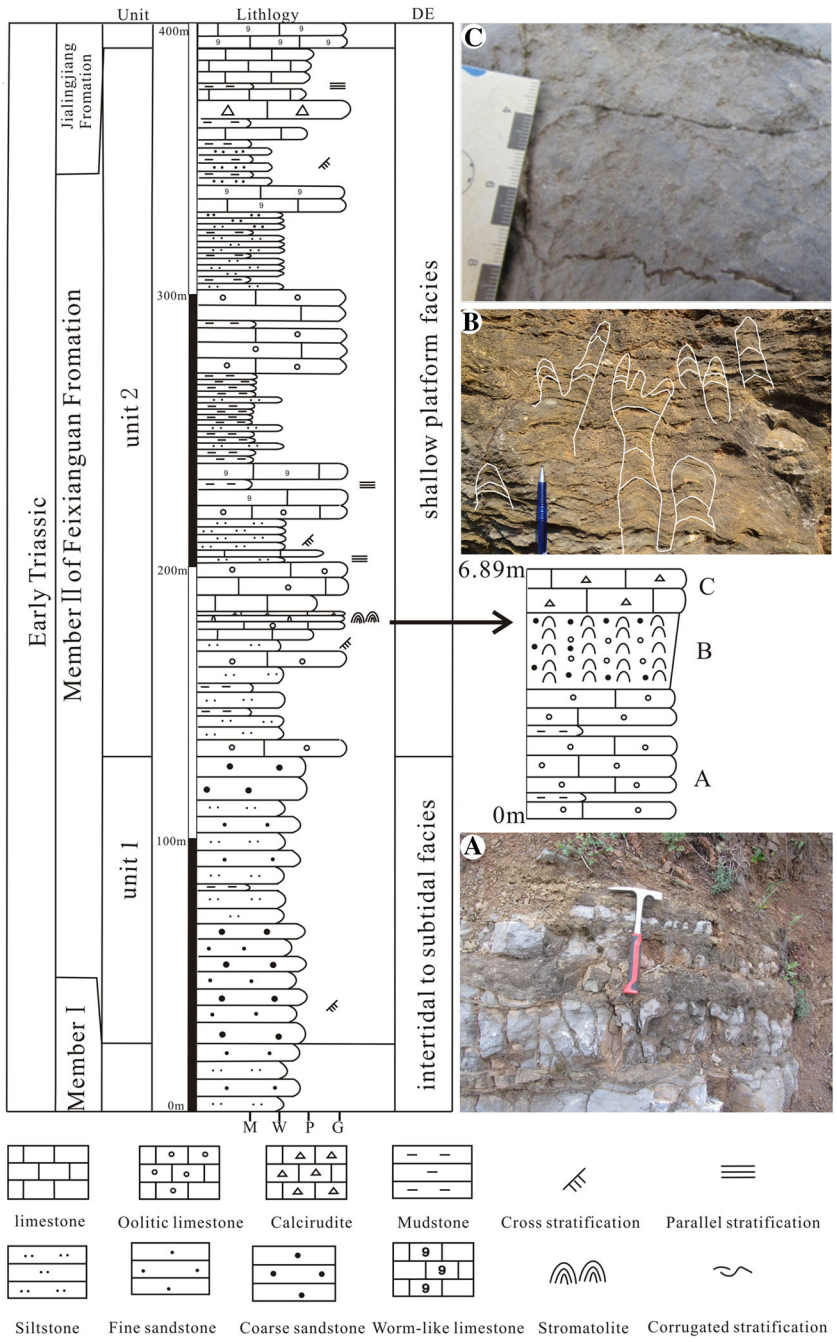

Fig. 2 Lithology and palaeoenvironmental analysis of Member II of the Feixianguan formation at the logged section. Note the described stromatolite occurs at the middle part of unit 2(*black arrow* **B**)

limestone and mudstone (Fig. 2A), indicating deposition by episodic storms. The oolitic deposits (Fig. 2B) consist of dark to light grey, medium to thin bedded, granular and micritic limestone. The muddy limestone has a stromatolitic texture and contains the stromatolitic deposit (Fig. 2B) that is the focus of this study. Large amounts of bioclastic debris are present in the stromatolites, mainly bivalves and foraminifera. The stromatolites are covered by calcirudite (Fig. 2C). The calcirudite is rounded with good resistance, well sorted and cross-bedded, and represent storm-flow deposits. Thus, both lithofacies and palaeoecology suggest that Unit 2 overall represents an open, shallow platform to proximal ramp environment (Shi et al. 2010). Integration of the information on sedimentary facies and palaeoecology indicates that the Feixianguan Formation in the Xingyi area records a deepening-upward succession.

Conodont biostratigraphy was used to determine the age of the stromatolites. Unfortunately, conodonts were not recovered from near the stromatolites. Near the stromatolite-bearing horizons, however, the bivalves *Claraia* sp., *Unionites* sp., *Claraia longyanensis* Chen and *Claraia* cf. *aurita* (Hauer) were found at the top of Member I of the Feixianguan formation. These taxa indicate an early Dienerian age (Wu 1985; Yang et al. 1986; Tong et al. 2005). The conodonts *Lonchodina nevadensis* Mülleri, *Neohindeodella triassica* Mülleri, and *Lonchodina* cf. *mülleri* Tatge were recovered from the top of Member II of the Feixianguan Formation and the bottom of Member I of the Jialingjiang Formation. Moreover, the conodonts *Pachycladina* and *Parachirognathus* were found at the top of Member I of the Jialingjiang Formation. These taxa indicate that the top of Member II of the Feixianguan Formation is of early Olenekian age (Tong et al. 2005; Ji et al. 2011; Yan et al. 2013). The stromatolite-bearing horizon is present in the upper part of Member II (Fig. 2). The bivalves *Bakevellia* sp. was detected 55 m stratigraphically above the stromatolites. To summarize, the stromatolites may be of middle or late Dienerian age.

Methods

Polished slabs and petrographic thin sections were prepared to examine the internal fabrics and diagenetic features of the stromatolites. Fresh samples and polished chips were made separately for microanalysis under the scanning electron microscope (SEM). Freshly broken samples were cleaned with deionized water, immersed in 0.5 % hydrochloric acid for 3–5 h, and rinsed again with deionized water and ethyl alcohol. Samples for SEM analysis were polished with 200-mesh diamond dust prior to chemical etching and cleaning. Samples were gold-coated using a Hitachi-SU4800 FEGSEM. Elemental mapping of energy-dispersive X-ray spectrometry (EDS) analysis was performed with a Shimadz EPMA-1600 at the Southwest China Supervision and Inspection Center of Mineral Resources, Ministry of Land and Resources at the Chengdu Center of the China Geological Survey. Fluorescent imaging analysis was performed to assess the distribution of residual organic matter using a Zeiss Microscope at the State Key Laboratory of Oil and Gas Reservoir Geology and Exploitation at the Chengdu University of Technology. Recent studies have demonstrated that different colours of fluorescent light represent different levels of organic matter. A rock containing abundant organic matter will fluoresce strongly in both green and purple excitation light (Luo et al. 2014). In contrast, if a rock has little or no organic matter, the rock will weakly or not fluoresce (Cuif et al. 1990; Reitner and Neuweiler 1995; Russo et al. 1997, 2000; Mastandrea et al. 2006). In this study, the terminology and methods for documenting stromatolite microfabrics follow Shapiro (2000), who described microbial fabrics at three different scales.

Results

Mega-, macro- and mesostructures of Xingyi stromatolites

The substrate of the stromatolites is an oolitic limestone with a granular texture. The limestone is 20–30 cm thick and contains bioclasts. The matrix is dominated by superficial ooliths about 1 mm in size. The ooliths become larger gradually upward. Gastropod shell fragments 1–2 cm in size are mainly recrystallized as calcite.

The capping facies of the stromatolites is calcirudite (Fig. 2C) that has a thickness of more than 50 cm. Calcirudite with irregular appearance 2–3 mm in size, and are poorly sorted. Both the oolitic limestone and the calcirudite contain abundant, irregularly shaped grains with few fossil fragments. In contrast, the stromatolites are dominated by light-coloured and dark laminae with few grains.

Stromatolites with columnar structures formed by alternations of light-coloured and dark laminae are distinct from the surrounding rocks (Fig. 2B). The columnar structures are 8–25 cm high and 3–6 cm long. In cross-section, the stromatolites are discrete hemispheroids in shape (Fig. 3A, B). These hemispheroids are stacked vertically to form the columnar structures. In polished slabs, the concentric laminae are 1–2 mm thick (Fig. 3B).

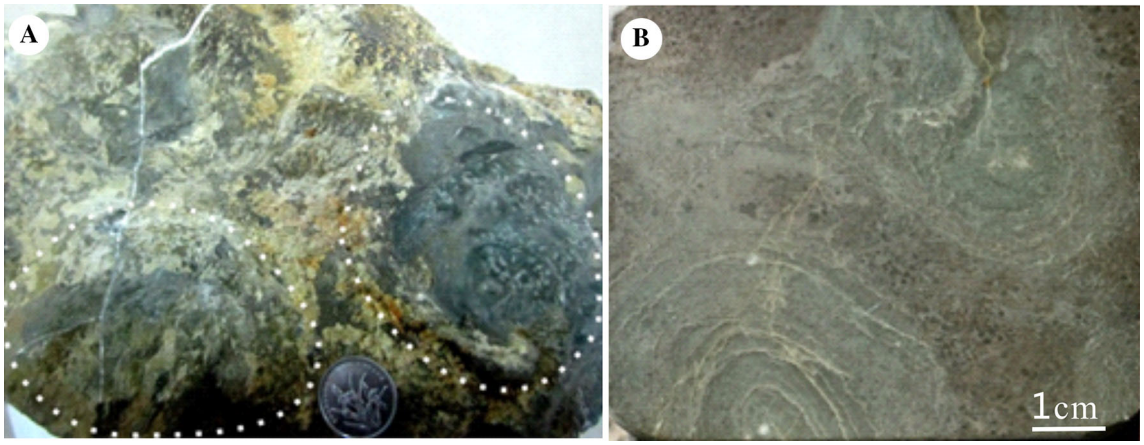

Fig. 3 Polished surfaces and field photos show stromatolite of Member II of the Xingyi formation. **A** Field photos showing note columns preserved as rounded reliefs (*white curve*). **B** Polished surfaces showing spheroidal structures

Stromatolite microstructures

Microscopic observation showed that the stromatolites have a columnar structure, characterized by undulating laminations with few grains (Fig. 4A, B). The grains, which do not have oolitic envelopes and are small in size, are different from the grains in inter-stromatolites (Fig. 10B, D).

Stromatolitic laminae can be divided into two categories, dark and light, on the basis of colour. The boundaries of these laminae are not complete. Dark grey laminated layers, which have an average thickness of 400 μm, are mainly composed of dark grey micritic calcite and abundant filamentous structures (Fig. 4A, B). There are two types of filamentous structure: upright and prostrate. The upright structures, which are usually perpendicular to the dark laminae and grow straight upward, possess three main features: they have microsparitic cores and micritic walls, appear as unbranched tubes in outline, and do not possess nodes. The diameters of the upright filamentous tubes range from 5 to 15 μm with the mean value of 8 μm, based on the measurements of 43 individuals.

The prostrate filamentous structures are strongly curved and are, in general, distributed nearly parallel to the thin laminae (Fig. 4D). Individual filamentous structures are composed of microsparite in the core, with walls defined by micrite (Fig. 4D). The diameters of the prostrate filamentous structures are similar to those of the upright tubes. In contrast, the light-coloured laminae with poor lateral continuity, which are usually composed of microsparite, are 2–8 mm thick (Fig. 4D). Under the fluorescent microscope, the dark laminae showed strong fluorescence under blue excitation light (Fig. 5A, B). Moreover, the microsparite areas within dark laminae that lack well-preserved filaments (Fig. 5A, B) also showed strong fluorescence. In contrast, the light-coloured laminae have very weak fluorescence (Fig. 5C, D); however, the filamentous tubes fluoresce the same colour as the micritic cement (Fig. 5D). Strong fluorescence indicates the presence of abundant organic matter in these microfabrics (Cuif et al. 1990; Reitner and Neuweiler 1995; Russo et al. 1997, 2000; Mastandrea et al. 2006).

Filamentous microfossils

Under SEM, well-preserved filamentous microfossils are common in the dark laminae. This is a distinct difference from the substrate of the stromatolites, which contains only microcrystalline calcite. The filamentous microfossils are characterized by being flexuous and unsegmented and having unbranched tubular outlines (Fig. 4A–C). Each individual is delimited by micritic walls, appear as short columns in the plane (Fig. 4A) and show a few pores in cross-section (Fig. 4D). The diameter of the filamentous microfossils ranges from 5 to 18 μm and the wall thickness ranges from 1 to 3 μm, based on measurements of 19 individuals. In contrast, the filamentous structures are 20–150 μm long, with the mean value of 35 μm. Irregularly shaped polyhedral (Fig. 6B) and tabular calcite (Fig. 6A, C) are associated with thin tubes (Fig. 6B).

Smaller bacilli

Under SEM, it can be seen that smaller bacilli are mostly aggregated locally to form irregular rod-like aggregates (Fig. 7A, B) and reticular rounded pits (Fig. 7D). These structures are commonly present in the light-coloured laminae of stromatolites. The diameter of the irregular and meshed rod-like aggregates (Fig. 7A) ranges from 2 to 8 μm, with the mean value of 5 μm based on

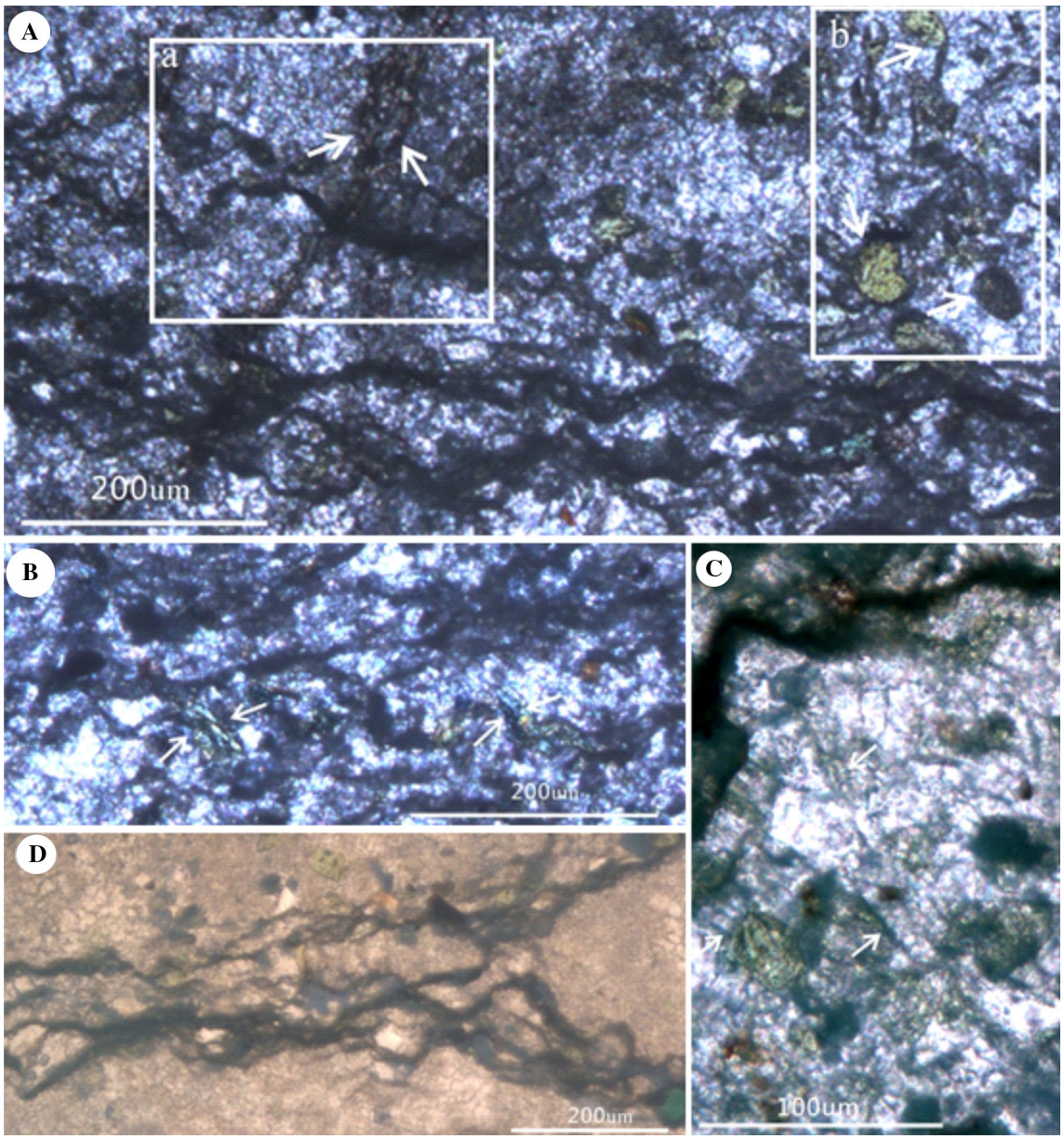

Fig. 4 Photomicrographs show the Xingyi stromatolite. **A–C** Showing the well-preserved filamentous tube colony comprising individual upright filaments in life position (*white arrows*), **A**-*b* Showing grain packstone caps the laminated stromatolite. **D** Showing prostrate filament and fenestrae in dark laminae

measurements of nine individuals. Reticular rounded pits (Fig. 7C, D) were also commonly observed in the light-coloured laminated layers of stromatolites. The reticular rounded pits (Fig. 7D) are circular in outline and 0.8–1.5 μm in diameter with an average diameter of 1.2 μm, based on measurement of 12 individuals. Both these pits and irregular mesh consortia are formed of smaller bacilli, but are interwoven in different ways. The smaller bacilli (Fig. 7B, D) are 0.1–0.2 μm in diameter with the mean value of 0.15 μm, based on measurements of 19 individuals. The smaller bacilli are 0.2–1.5 μm in length with the mean value of 0.35 μm, based on measurements of 31 individuals. The smaller bacilli split continuously, as shown by cells that are Y-shaped in outline (Fig. 7B, D).

Coccoid-like spheroids and oval algae

Small spheroidal structures are common in the dark-coloured laminae of the stromatolites. Some spheroids are globular in outline, 10–12 μm in diameter, and are formed of clusters of many minute rhombic calcite crystals (Fig. 8A). Under SEM, well-preserved oval algae (Fig. 8B–

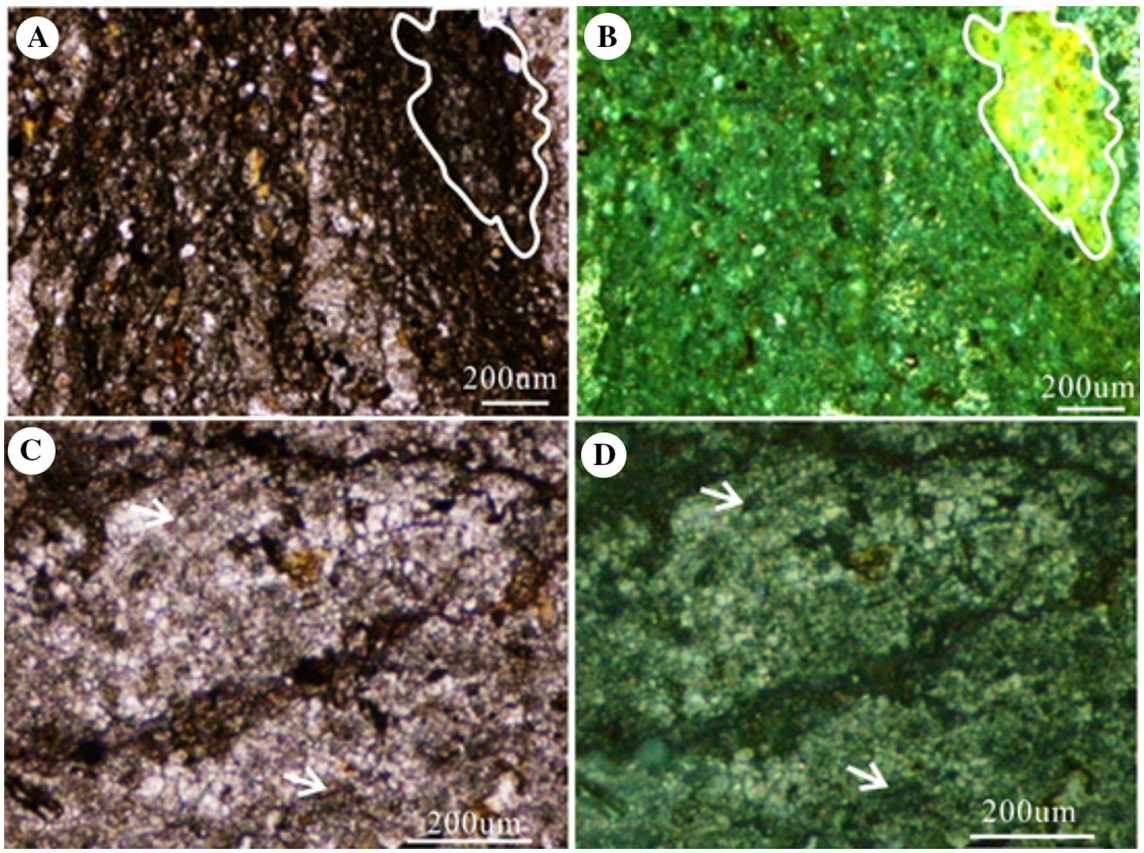

Fig. 5 Filament-rich and clotted fabric areas in dark laminated layers of stromatolite in transmitted light and fluorescent light. **A** The prostrate filamentous tube in the dark laminae. **B** The same area as that in view **A** show the dark laminae showed a strong fluorescence under blue exciting light. **C–D** Another view of clotted fabrics in the bright laminae of stromatolite. Filamentous tube (*white arrows*). **D** Coarsely sparry calcite cementation was poorly responded to fluorescent light. Filamentous tube (*white arrows*) was similar to micrites cementation

D) are commonly present in the dark laminated layers of stromatolites. These algae are markedly different from the spheroidal structures. The oval algae are cystic (Fig. 8C, D) in outline and 20–60 μm in size, with the mean value of 35 μm based on measurements of 22 individuals. These algae always have verrucae that are 0.2–1 μm in size (Fig. 8C). Some have a smooth surface with no folds or little folding, and sometimes bear a small protuberance (Fig. 8D).

Extracellular polymeric substance and associated polyhedrons

Another feature typifying the cyanobacteria is the common presence of extracellular polymeric substance (EPS) and associated polyhedrons (Po) (Fig. 9A–D). These EPS form fibrous structures, which cover or around the organic matter (Fig. 9A, C). Po cover or around the EPS (Fig. 9A, D).

Framboidal pyrite

Pyrite framboids are also common in the stromatolite microstructures. The framboids coexist with sparry calcite within stromatolitic laminae, have strawberry-shaped, globose outlines (Fig. 10A–D) and are formed of smaller euhedral pyrite crystals. The majority of the smaller euhedral pyrite crystals (more than 70 %) have a spheroplastic appearance (Fig. 10B) and a few (less than 30 %) are tetrahedral in shape (Fig. 10D). The size of the framboids is 4–18 μm with the mean value of 10 μm, based on measurements of 29 specimens. The framboids commonly occur in clusters, and sometimes as loose groups.

Authigenic quartz

Quartz crystals are also obvious in the stromatolite microstructures. The crystals coexist with sparry calcite within the stromatolitic laminae. The crystals have subidiomorphic outlines and pronounced crystal structures on the surfaces (Fig. 10E, F). The crystal size is 2–6 μm, with the mean value of 4 μm based on measurements of 27 crystals. The quartz (Fig. 10E, F) are scattered in the stromatolite laminae and not concentrated to form layers or horizons. They show no signs of abrasion, which are

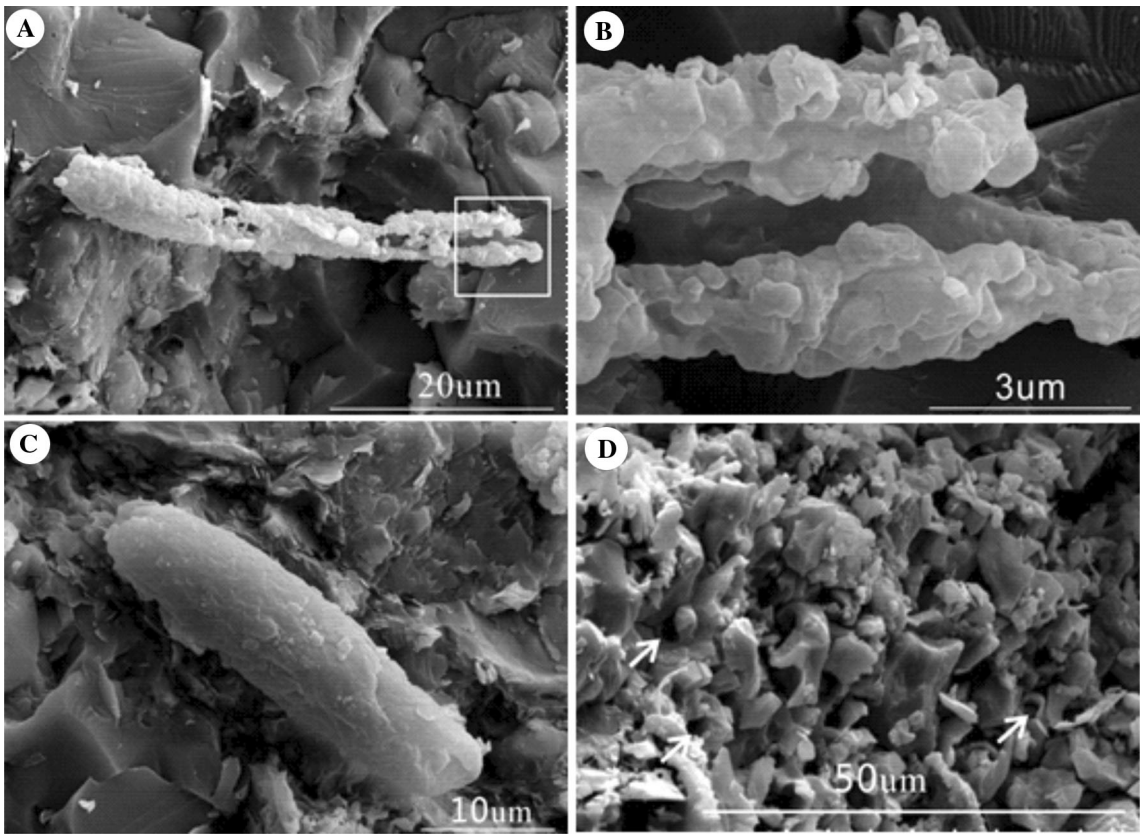

Fig. 6 SEM images of filamentous structures detected in dark laminae of the Xingyi stromatolites. **A** Thin tubular filament was cementated by calcite. **B** Close-up of *boxed area* in view **A** show filamentous microfossils and polyhedron. **C** Filamentous tube associated with tabular calcite. **D** Few amount of pores in cross-section

typical features of detrital quartz grains. As these crystals show no indications of transported, they are probably authigenic in origin.

Inter-stromatolite microstructures

The spaces between the stromatolites are dominated by grains (Fig. 11A–D) that fall into two size categories. The diameter of the smaller grains is 50–120 μm with the mean value of 80 μm, based on measurements of 49 individuals. Although fragmented relicts are observed, individual primary grains are difficult to distinguish because the smallest grains have been recrystallized and strongly calcitized (Fig. 11B). Other particles are oncoids composed of an irregular cortex and nuclei (Fig. 11B, C). Grapestone is characterized by multiple nuclei and common envelopes (Fig. 11C). The diameter of the oncoids is 200–600 μm with the mean value of 400 μm, based on measurements of 52 grains. Some oncoids are infilled by pyrite (Fig. 11D), which occur only within the cortex and do not appear outside the cortex. Small gastropods occur sporadically among the grains (Fig. 11D).

Discussion

Biogenic origin of stromatolites

A large numbers of evidences show that various microbial colonies are present in different stromatolite laminae. The metabolic processes of these microbes interact to promote the formation of stromatolites (Dupraz et al. 2004). Microorganisms can be divided into six typical functional groups on the basis of their roles in rock diagenetic processes (Dupraz and Visscher 2005; Visscher and Stolz 2005; Dupraz et al. 2009). These groups are as follows. (1) Oxygenic phototrophs (cyanobacteria) are major primary producers and use light energy to fix CO_2. Filamentous cyanobacteria and spherical bacteria play an important role in the capture and cohesion of sedimentary grains with EPS) and biofilms. (2) Anoxygenic phototrophs such as purple and green sulfur bacteria use H_2S for photosynthesis. (3) Aerobic heterotrophic bacteria live by respiring oxygen and consuming organic matter. (4) Fermenting bacteria use organic matter or sulfur compounds in their metabolism. (5) Anaerobic heterotrophs (a major type is sulfate-reducing bacteria; SRB) consume organic matter,

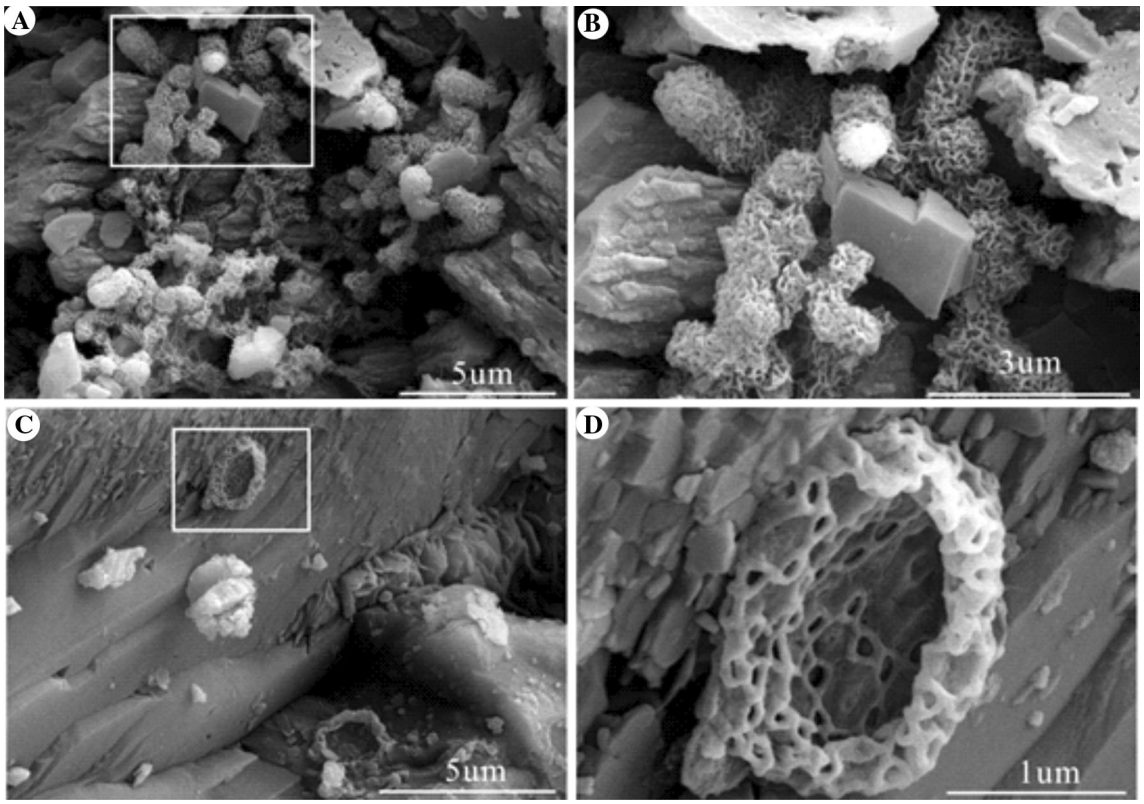

Fig. 7 SEM images of Smaller bacilli detected in dark laminae of the Xingyi stromatolites. **A** Irregular rod-like aggregates. **B** Close-up of *boxed area* in view **A** showing irregular rod-like aggregates. **C** Reticular rounded pits. **D** Close-up of *boxed area* in view **C** showing reticular rounded pits and smaller bacillus is characterized by cells with "Y" in outline

including SO_4^{2-}, to yield HS^-. (6) Sulfide-oxidizing bacteria, which are inorganic chemical autotrophic bacteria, play an important role in fixing CO_2 and reducing sulfur. Studies of modern stromatolites have shown that all microbial groups together establish a semi-closed system in the stromatolites, which maintains the circulation of effective elements and the highest metabolic rate (Visscher et al. 1998; Dupraz et al. 2004). However, not all of these six microbial groups are found at the same time, because microbial metabolism within the microbial mat varies strongly from place to place (Reid et al. 2000; Baumgartner et al. 2006; Dupraz et al. 2009; Heindel et al. 2012; Voorhies et al. 2012). Biosignatures from ancient lithified examples are important for understanding the genesis and palaeoenvironmental implications of stromatolites in the geological past (Noffke and Awramik 2013). In this study, three key microbial groups, which were involved in the stromatolite accretion processes, were detected in the Xingyi stromatolites.

Oxygenic phototrophs in stromatolites

Upright and prostrate filamentous tubes are often present in the undulating laminae of the Xingyi stromatolites. Morphologically, these filamentous tubes are flexuous, unsegmented, unbranched tubes. Each individual has well-defined dark walls in longitudinal section (Fig. 4A–C, Fig. 5C, D, Fig. 6A–C) and are circular in transverse section (Fig. 6D). Each filamentous tube has a constant diameter. The external diameter of the filaments is 5–18 μm and the wall thickness is 1–3 μm. Considering these characteristics, it is concluded that the filamentous tubes are similar to the morphological group of tubiforms, which are non-fan forms of cyanobacteria (Flügel 2010; Martin 2010; Reitner and Neuweiler 1995; Riding 1991).

Spheroidal balls, which are formed of clusters of many minute rhombic calcite crystals, are similar to small ball-like objects reported from Late Triassic stromatolites (Mastandrea et al. 2006; Perri and Tucker 2007) and modern examples of mineralized capsules from Lake Vai Si'I, Tonga (Kaźmierczak and Altermann 2002) in both outline and size.

Oval algae with no plastic sheath and single cell have a mean diameter of 25 μm, and are often observed in Xingyi stromatolites. Oval algae are a type of cyanobacteria that have been reported from Late Triassic limestone (Liu 1982; Liu and Liu 1984).

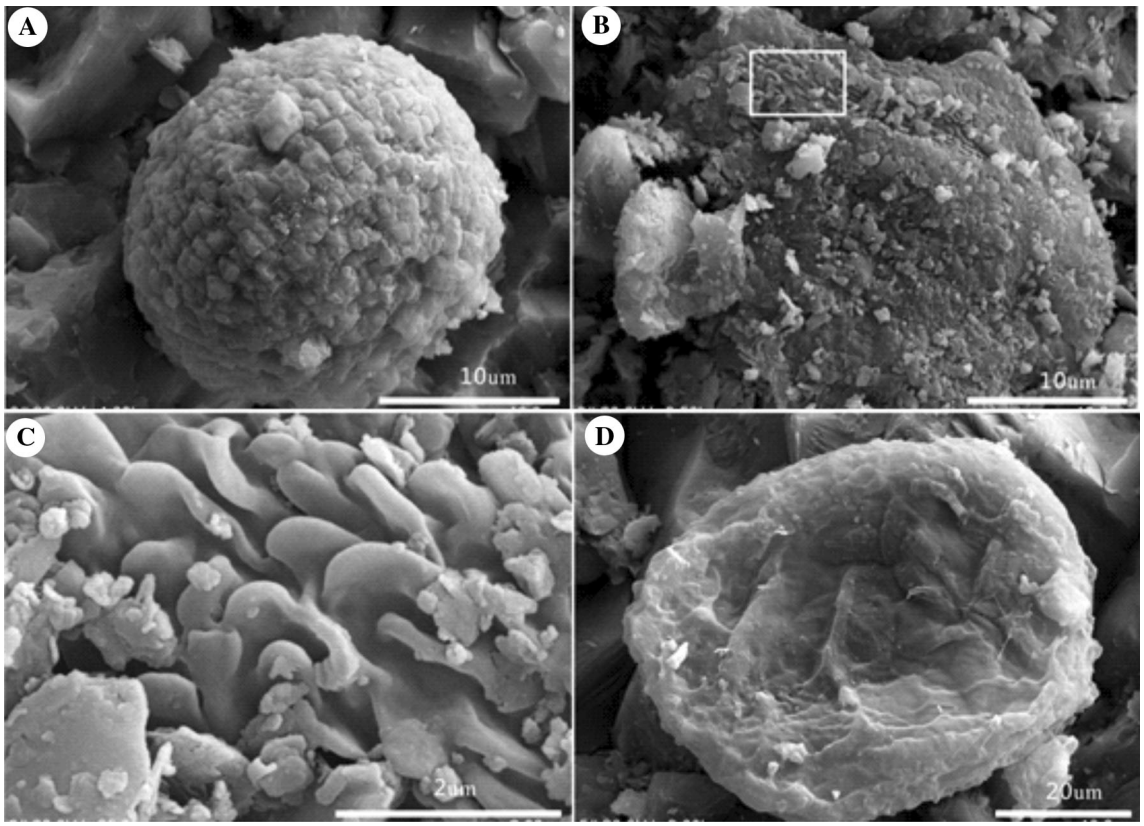

Fig. 8 SEM images of coccoid-like spheroids and oval algae are detected in dark laminae of the Xingyi stromatolites. **A** Spheroid balls are globular in outline and lustered by many minute rhombic limestone crystals. **B** The oval algae always have verruca. **C** Close-up of *boxed area* in view **B** verruca. **D** The oval algae have smooth surface with no fold or little fold, but have a small protuberance

Regardless of the classification of these different cyanobacteria, which coexisted in the dark laminae, the dark laminae usually show strong fluorescence under the fluorescent microscope (Fig. 5B–D), indicating that these layers are rich in organic matter, as in other stromatolites (Cuif et al. 1990; Reitner and Neuweiler 1995; Russo et al. 1997, 2000; Mastandrea et al. 2006; Luo et al. 2014). Modern research has shown that fossilized cyanobacteria may have been the primary producers (Kaźmierczak et al. 2011; Voorhies et al. 2012) that built the Xingyi stromatolites. In the Xingyi stromatolites, oxygenic phototrophs may have contributed to carbon fixation and oxygen production, which is favourable for growth of other microbial groups (Kaźmierczak et al. 2011; Voorhies et al. 2012). It has been documented that some filamentous cyanobacteria can thrive in low-O_2 environments and carry out primary production by anoxygenic photosynthesis (Voorhies et al. 2012); however, the material in that study was not lithified. Thus, cyanobacterial fossils may indicate the presence of oxygenic phototrophs rather than anoxygenic phototrophs in the Xingyi stromatolites. This view has been widely adopted to explain the Permian–Triassic boundary microbialites and Lower Triassic microbialites with abundant filamentous cyanobacteria (Reid et al. 2000; Decho et al. 2005; Chen et al. 2012; Luo et al. 2014).

Sulfate-reducing bacteria in stromatolites

Many evidences show that sulfate reduction may also have been an important mechanism of carbonate precipitation in these fossilized structures (Visscher et al. 2000). Although bacterial sulfate reduction in the subsurface environment (Wright and Wacey 2005) has not been directly observed, there are three pieces of evidence indicating the presence of SRB in the Xingyi stromatolites. First, framboidal pyrite is a common type of pyrite in sedimentary rocks, and is composed of many tiny crystallites that have similar size and composition (Rickard 1970; Wilkin and Barnes 1996, 1997). Microcrystalline pyrite can form a variety of structures (Butler and Rickard 2000; Ohfuji and Rickard 2005), including spheroidal, pentagonal like spheroplasts, hexahedra and tetrahedra. Studies show that the formation of framboidal pyrite is related to the presence of SRB (Berner 1984; Coleman et al. 1993). The H_2S generated by SRB play an important role in formation of framboidal pyrite (Wilkin and Barnes 1997; Grimes et al. 2001).

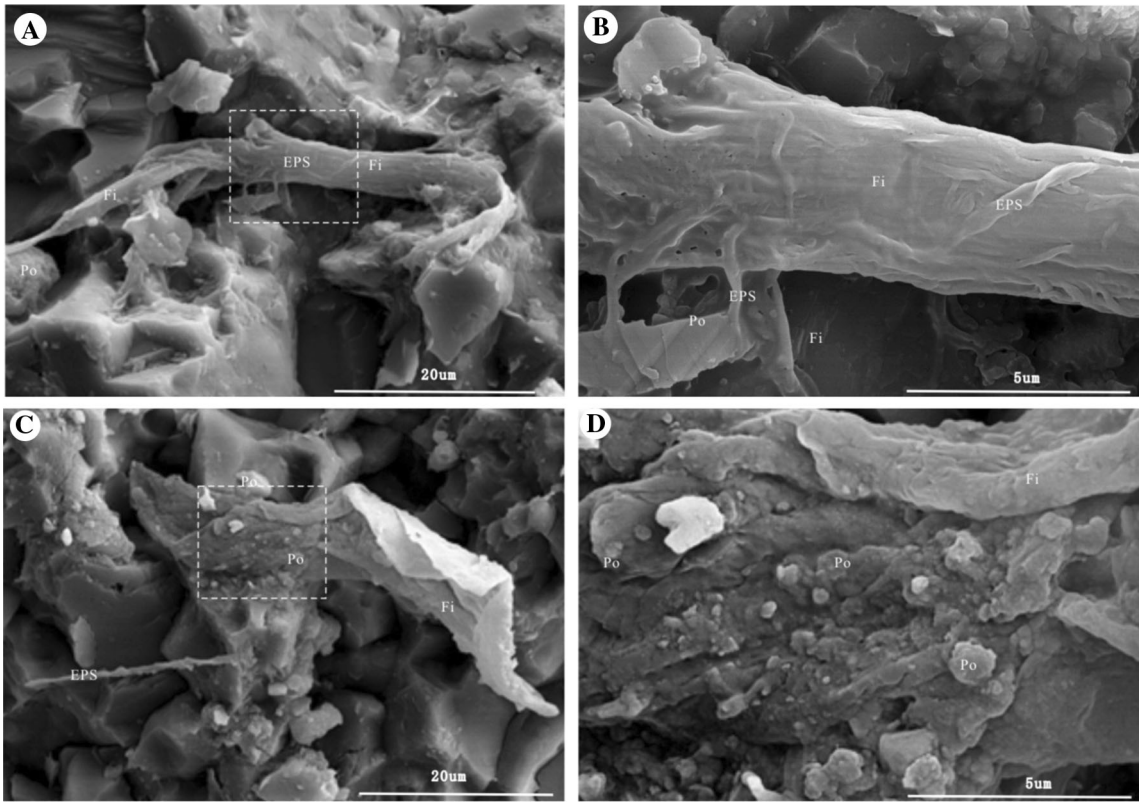

Fig. 9 SEM images of extracellular polymeric substance (EPS), associated polyhedrons (Po) and filameatous bacteria relies (Fi) **A**–**D** Extracellular polymeric substance (EPS), associated polyhedrons (Po) and filamentous bacteria relies (Fi) in dark lamina. **B** Close-up of *boxed area* in view **A**. **D** Close-up of *boxed area* in view **C**

Therefore, the presence of framboidal pyrite indicates that SRB were present in the Xingyi stromatolites.

Second, authigenic quartz grains are abundant in stromatolitic laminae. Although sources of silica are common, an acidic environment is necessary for formation of authigenic quartz crystals (Campbell et al. 2002; Peckmann and Thiel 2004; Joye et al. 2010), in which bacterial sulfate reduction and sulfide oxidation play an important role (Friedman and Shukla 1980). It should also be noted that the possibility that the euhedral quartz may have had a volcanic origin cannot be ruled out, because morphologically identical authigenic quartz produced by volcanic eruptions has been recorded in Permian–Triassic rocks in South China (Yin et al. 1992).

Third, in the Xingyi stromatolites, tabular calcite and calcite in the shapes of irregular polyhedra, which are composed of many nanoparticles, are found closely associated with EPS (Pacton et al. 2010). EPS (Fig. 9A, B) and SRB have a crucial role in calcium carbonate precipitation (Spadafora et al. 2010; Perri and Spadafora 2011; Perri et al. 2012). EPS can serve as a template to induce calcite formation directly from solution, and can be regarded as an alveolar organic network within which calcite precipitation can be initiated (Bontognali et al. 2010). In addition, SRB disintegrate EPS, consuming sulfate in the process; this raises the alkalinity of the microenvironment, which is favourable for carbonate precipitation (Dupraz et al. 2004, 2009).

EDS analysis of two different lithified cyanobacteria and calcite (Fig. 12A, B) suggests that the lithified cyanobacteria and EPS are rich in Mg and Ca with a small percentage of Si (Fig. 12B). This was probably caused by subsequent Ca incorporation within the previously formed Si–Mg phase that was encapsulated by the EPS matrix. Calcified EPS produced by microbial communities is important in the development and lithification of stromatolites (Dupraz et al. 2004, 2009; Spadafora et al. 2010; Glunk et al. 2011). SRB, supersaturated $CaCO_3$ and high alkalinity of the microenvironment are the main factors required for stromatolite lithification (Glunk et al. 2011).

Possible anoxygenic phototrophs in stromatolites

Smaller aggregates of bacilli such as irregular rod-like aggregates (Fig. 7A, B) and reticular rounded pits (Fig. 7D) are common in the undulating laminae of the Xingyi stromatolites. Smaller bacilli split to form Y-shaped structures, which combine together to form three-dimensional reticular aggregates. This Y-shaped structure is

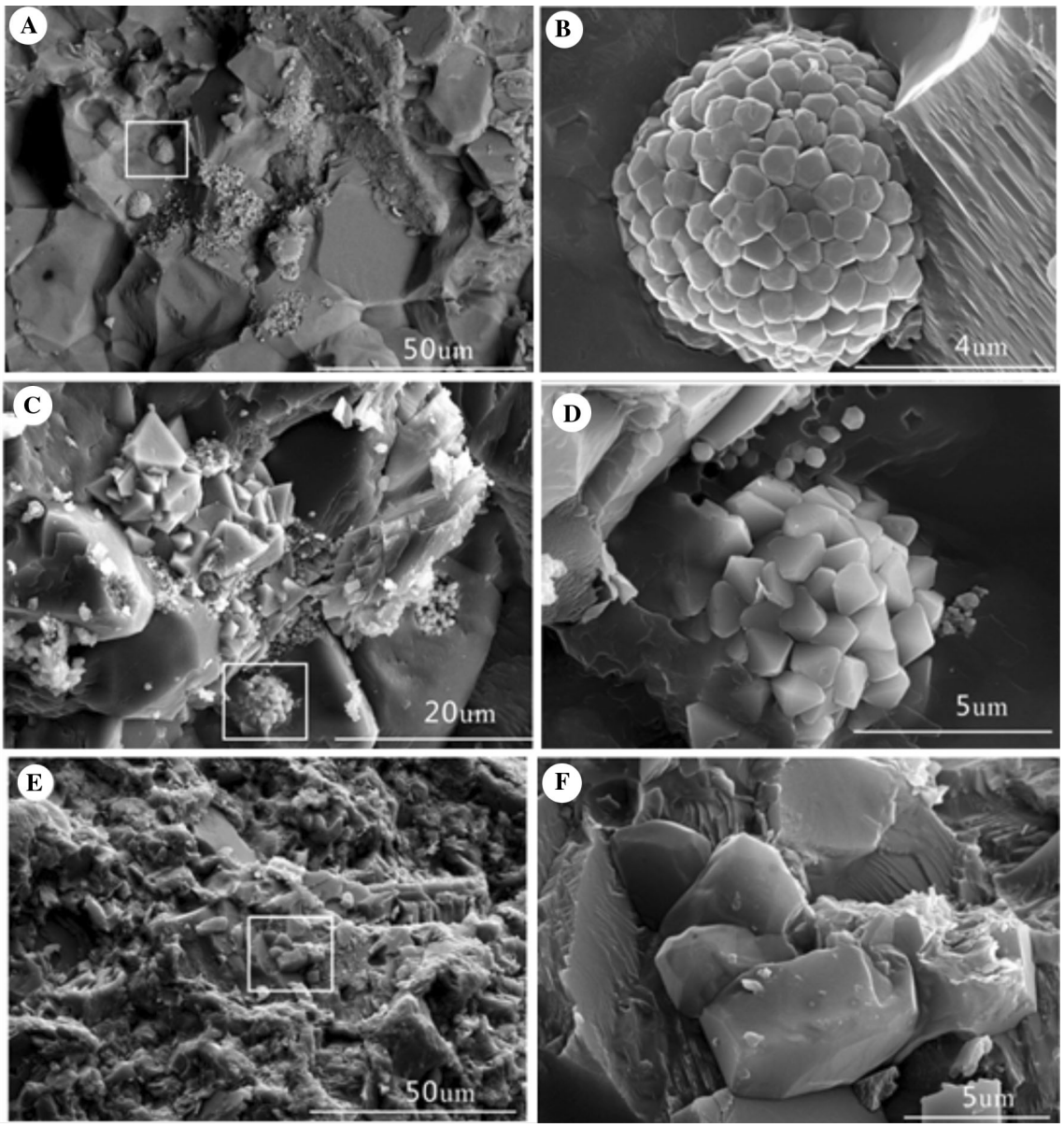

Fig. 10 SEM images of framboidal pyrite and authigenic quartz detected in dark laminae of the Xingyi stromatolites. **A** Framboidal pyrite plexus. **B** Close-up of *boxed area* in view **A** showing framboidal pyrite have the appearance of like spheroplast. **C** Framboidal pyrite plexus. **D** Close-up of *boxed area* in view **C** showing framboidal pyrite have the appearance of tetrahedron. **E** Authigenic Quartz crystals. **F** Close-up of *boxed area* in view **E**

similar to the microscopic structure of *Pelodictyon clathratiforme* (Pfennig 1968). These bacilli are smaller than *P. clathratiforme*, which is 0.7–1.2 µm in width and 1.5–2.5 µm in length; however, the aspect ratio of the Xingyi bacilli and *P. clathratiforme* is the same, having a value of 2. From only this evidence, it is not possible to infer that the smaller bacilli and *P. clathratiforme* are of the same bacterial type. However, the bacilli were involved in the formation of the stromatolites, as demonstrated by the capture or adhesion of microcrystalline particles in the bacterial aggregates (Fig. 7B, D).

There have been few detailed studies of geomicrobial taxonomy, in contrast to the large amount of work that has been conducted on geomicrobial ecology (Chen et al. 2014). The smaller bacilli cannot be definitely identified as *P. clathratiforme*, but there is also no evidence that they were not. *P. clathratiforme* is one of the Chlorobiaceae (Pfennig 1968), which are frequently found in shallow estuarine habitats such as closed bays and lagoons (Caumette 2011). This organism grows in exposed mud containing H_2S, stagnant water and hot springs (Pfennig 1977, 1978) and carries out photosynthesis using H_2S.

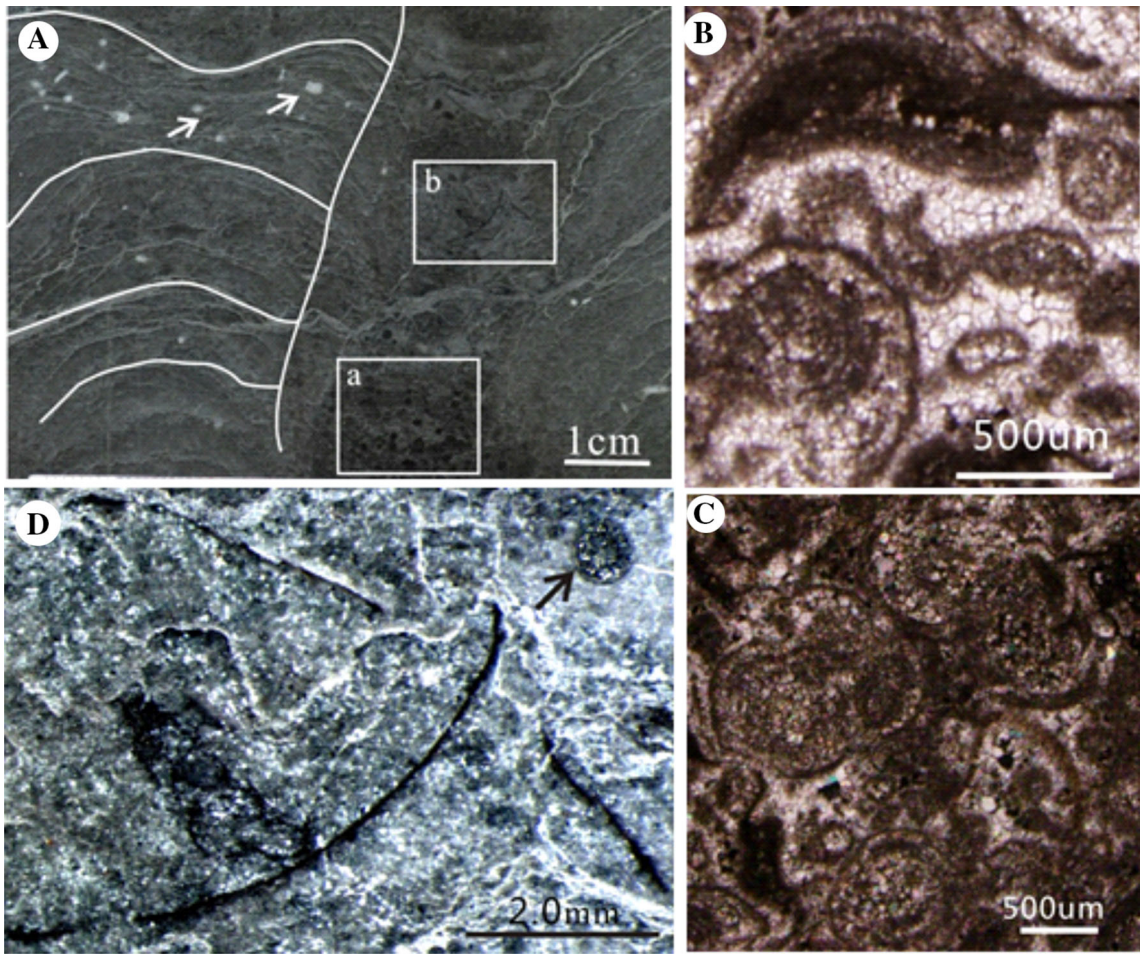

Fig. 11 Polished surfaces and microscopic photos show the parts of interstromatolite. **A** Inter-stromatolite facies is dominated by oncoids, the geode of gypsum or salt (*White arrow*) scattered in the stromatolite. **B** Close-up of *boxed area* in view of **A**-*a* showing grain consisting an irregular micrite clots. **C** Close-up of *boxed area* in view of **A**-*a* showing grapestones and lumps. **D** Close-up of *boxed area* in view of **A**-*b* showing shell fragments of bivalves. oncoids is filled by pyrite (*Black arrow*)

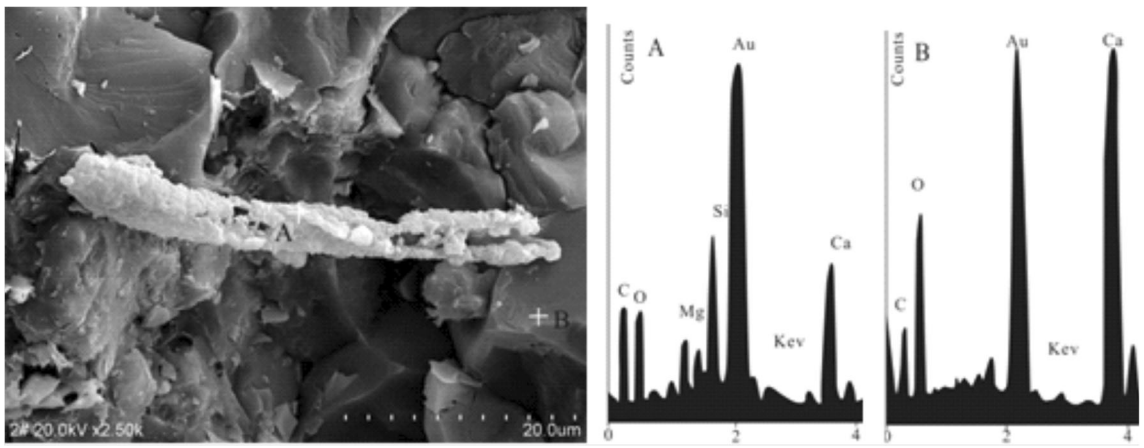

Fig. 12 EDS analytical results of two different components of caclite grains in the Xingyi stromatolites. *White* cross corresponds to analysing point. Element Au indicates goad coating of samples. **A** Flamentous tubes that showed a composition of Ca and Mg caclite (indicated by EDS spectrum in **A**), with low percentage of element Si. **B** Caclite grains, which showed high percentage of element Ca incomposition (indicated by EDS spectrum in **B**)

These fossils that resemble *P. clathratiforme* probably represent anoxygenic phototrophs in the Xingyi stromatolites.

Other important microbial components, such as aerobic heterotrophs and sulfide-oxidizing bacteria, were not identified in Xingyi stromatolites. Two major microbial functional groups, oxygenic phototrophs indicated by fossilized filamentous cyanobacteria and SRB represented by framboidal pyrite, are obvious in the dark laminae of the Xingyi stromatolites. These remains might represent the most active microbial communities in the stromatolite ecosystem, and may have contributed to the accretion of stromatolites. In addition, another possible microbial functional group, anoxygenic phototrophs represented by lithified structures resembling *P. clathratiforme*, may have been present in the Xingyi stromatolites. Even if this functional group was not present, the smaller bacilli were involved in stromatolite formation. To summarize, the Xingyi stromatolites are biogenic in origin.

Implications for Early Triassic stressed marine environments and microbial proliferation

Early Triassic microbialites, including stromatolites, thrombolites and other forms, are characteristic of P–Tr successions in shallow marine facies around the world (Kershaw et al. 2012). Although the debate on the genesis of P–Tr microbialites still continues (Kershaw et al. 2007, 2012; Mata and Bottjer 2012), microbes existed widely in various niches of the post-extinction oceans (Xie et al. 2005; Baud et al. 2007; Ezaki et al. 2012; Chen et al. 2014; Heindel et al. 2015; Luo et al. 2014). Sun et al. (2012) tested oxygen isotopes from Early Triassic conodonts, and estimated the temperature of sea water to have been up to 40 °C during the late Smithian. In contrast, the temperature of sea water during the late Permian was 25 °C (Joachimski et al. 2012; Sun et al. 2012). This warmer temperature would have been favourable for flourishing of cyanobacteria. In addition, significant quantities of nutrients (such as Fe, N, and P) are deposited in the sea after volcanic eruptions (Algeo and Twitchett 2010; Lindenthal et al. 2012; Ayris and Delmelle 2012), which would have also contributed to cyanobacterial blooms (Abraham et al. 2000; Duggen et al. 2010; Olgun et al. 2011). Moreover, after the Permian mass extinction, a lack of metazoan interference resulted in proliferation of cyanobacteria (Schubert and Bottjer 1992, 1995). The occurrence of Dienerian stromatolites in the northwest Nanpanjiang Basin confirms the proliferation of microbialites in the Dienerian, which was the second stage of four distinct growth episodes of enhanced microbialite growth during the Early Triassic (Baud et al. 2007). Microbial proliferation during the Early Triassic is thought to indicate an unhealthy trophic structure in the marine ecosystem and environmental devastation, which delayed biotic recovery following the P–Tr crisis (Chen and Benton 2012). The devastated, unstable marine ecosystem in the Dienerian is also indicated by the large shifts in carbon isotopic values in the Nanpanjiang Basin (Tong et al. 2002, 2007; Payne et al. 2004). Both the Yangtze platform and the Nanpanjiang Basin preserve large $\delta^{13}C$ fluctuations (3–8 %) during the Griesbachian to late Smithian time interval (Huang et al. 2012, Song et al. 2012, Song et al. 2014). This carbon isotope positive excursion indicates burial of large amounts of organic matter during the Dienerian. The lack of Early Triassic land coal deposits indicates that terrestrial plants made very little contribution to the organic burial rate; instead, cyanobacteria were extremely important for the organic burial rate. Cyanobacteria have been confirmed to occupy an important position in the ocean carbon cycle (Kolber et al. 2001). As a result, the occurrence of the Xingyi stromatolites is consistent with the earlier view that microbes proliferated in time and space after the severe P–Tr mass extinction (Pruss et al. 2006; Baud et al. 2007).

Conclusions

1. The Xingyi stromatolites show typical stratified columnar structures formed of crinkled laminae. Dark-coloured laminae are composed of upright and prostrate filamentous structures. Upright filamentous structures show a straight-upwards growth fabric.
2. Two main microbial functioning groups, oxygenic phototrophs represented by lithified Cyanobacteria and probable SRB represented by framboidal pyrite, are distinct during the growth of stromatolites. Another possible microbial functional group, anoxygenic phototrophs represented by lithified remains similar to *P. clathratiforme*, may be present in the Xingyi stromatolites. The smaller bacilli that resemble *P. clathratiforme* were involved in the formation of stromatolites by capture or adhesion of microcrystalline particles. All of this evidence demonstrates that these Early Triassic stromatolites are biogenic.
3. The occurrence of the Xingyi stromatolites, corresponding to a second episode of microbial growth, reveals that post-extinction microbialites were widespread during the Dienerian.

Acknowledgments The authors wish to thank Yun Li, Chengdu University of Technology for her guidance and helpful suggestions in sample preparation and fluorescent imaging. Anonymous reviewers are thanked for their critical comments and constructive suggestions, which have improved greatly the quality of the paper. This study is supported by Guizhou Institute of the geological and mineral survey

project (No.12120114068101) and Luoping biota of special geological survey project (No.12120114068001).

References

Abraham ER, Law CS, Boyd PW, Lavender SJ, Maldonado MT, Bowie AR (2000) Importance of stirring in the development of an iron-fertilized phytoplankton bloom. Nature 407:727–730. doi:10.1038/35037555

Algeo TJ, Twitchett RJ (2010) Anomalous early triassic sediment fluxes due to elevated weathering rates and their biological consequences. Geology 38:1023–1026

Algeo TJ, Chen ZQ, Fraiser ML, Twitchett RJ (2011) Terrestrial–marine teleconnections in the collapse and rebuilding of Early Triassic marine ecosystems. Palaeogeogr Palaeoclimatol Palaeoecol 308:1–11

Awramik SM (1992) The oldest records of photosynthesis. Photosynth Res 33:75–89

Awramik SM (2006) Respect for stromatolites. Nature 441:700–701

Ayris P, Delmelle P (2012) Volcanic and atmospheric controls on ash iron solubility: a review. Phys Chem Earth 6:103–112

Baud A, Richoz S, Pruss S (2007) The Lower Triassic anachronistic carbonate facies in space and time. Glob Planet Chang 55:81–89

Baumgartner LK, Reid RP, Dupraz C, Decho AW, Buckley DH, Spear JR (2006) Sulfate reducing bacteria in microbial mats: changing paradigms, new discoveries. Sediment Geol 185:131–145

Berner RA (1984) Sedimentary pyrite formation: an update. Geochim Cosmochim Acta 48:605–615

Bontognali TRR, Vasconcelos C, Warthmann RJ, Bernasconi SM, Dupraz C, Strohmenger CJ (2010) Dolomite formation within microbial mats in the coastal sabkha of abu dhabi (united arab emirates). Sedimentology 57:824–844

Bottjer DJ, Clapham ME, Fraiser ML, Powers CM (2008) Understanding mechanisms for the end-Permian mass extinction and the protracted Early Triassic aftermath and recovery. GSA Today 18:4–10

Butler IB, Rickard D (2000) Framboidal pyrite formation via the oxidation of iron (ii) monosulfide by hydrogen sulphide. Geochim Cosmochim Acta 64:2665–2672

Campbell KA, Farmer JD, Des Marais D (2002) Ancient hydrocarbon seeps from the mesozoic convergent margin of california: carbonate geochemistry, fluids and palaeoenvironments. Geofluids 2:63–94

Caumette P (2011) Distribution and characterization of phototrophic bacteria isolated from the water of bietri bay (ebrie lagoon, ivory coast). Can J Microbiol 30:273–284

Chen ZQ, Benton MJ (2012) The timing and pattern of biotic recovery following the end-permian mass extinction. Nat Geosci 5:375–383

Chen ZQ, Chen J, Tong JN, Fraiser ML (2010) Marine ecosystem changes from the latest Permian to Middle Triassic in Qingyan area, Guizhou, Southwest China. J Earth Sci 21:125–129

Chen ZQ, Fraiser ML, Bolton C (2012) Early triassic trace fossils from gondwana interior sea: implication for ecosystem recovery following the end-permian mass extinction in south high-latitude region. Gondwana Res 22:238–255

Chen ZQ, Wang Y, Kershaw S, Luo M, Yang H, Zhao L (2014) Early Triassic stromatolites in a siliciclastic nearshore setting in northern Perth Basin, Western Australia: geobiologic features and implications for post-extinction microbial proliferation. Glob Planet Chang 121(10):89–100

Coleman ML, Hedrick DB, Lovley DR et al (1993) Reduction of Fe(III) in sediments by sulphate-reducing bacteria. Nature 361(6411):436–438

Cuif JP, Gautret P, Laghi GF, Mastandrea A, Pradier B, Russo F (1990) Recherche sur la fluorescence uv du squelette aspiculaire chez les démosponges calcitiques triasiques. Geobios 23:21–31

Decho AW, Visscher PT, Reid RP (2005) Production and cycling of natural microbial exopolymers (eps) within a marine stromatolite. Palaeogeogr Palaeoclimatol Palaeoecol 219:71–86

Duggen S, Olgun N, Croot P, Hoffmann LJ, Dietze H, Delmelle P, Teschner C (2010) The role of airborne volcanic ash for the surface ocean biogeochemical iron-cycle: a review. Biogeosciences Discuss 7:827–844

Dupraz C, Visscher PT (2005) Microbial lithification in marine stromatolites and hypersaline mats. Trends Microbiol 13:429–438

Dupraz C, Visscher PT, Baumgartner LK, Reid RP (2004) Microbe–mineral interactions: early carbonate precipitation in a hypersaline lake (eleuthera island, bahamas). Sedimentology 51:745–765

Dupraz C, Reid RP, Braissant O, Decho AW, Norman RS, Visscher PT (2009) Processes of carbonate precipitation in modern microbial mats. Earth Sci Rev 96:141–162

Ezaki Y, Liu JB, Adachi N (2003) Earliest Triassic microbialite micro- to megastructures in the Huaying area of Sichuan Province, South China: implications for the nature of oceanic conditions after the end-Permian extinction. Palaios 18:388–402

Ezaki Y, Liu JB, Nagano T, Adachi N (2008) Geobiological aspects of the earliest Triassic microbialites along the southern periphery of the tropical Yangtze Platform: initiation and cessation of a microbial regime. Palaios 23:356–369

Ezaki Y, Liu JB, Adachi N (2012) Lower triassic stromatolites in Luodian County, Guizhou province, South China: evidence for the protracted devastation of the marine environments. Geobiology 10:48–59

Farabegoli E, Perri MC, Posenato R (2007) Environmental and biotic changes across the permian–triassic boundary in western tethys: the bulla parastratotype, italy. Glob Planet Chang 55:109–135

Feng Z, Bao Z, Li S (1994) Lithofacies paleogeography of Early and Middle Triassic of South China. Sci geol sin 32:212–220 **(in Chinese)**

Flügel E (2010) Microfacies of carbonate rocks. Springer, New York, p 976

Friedman GM, Shukla V (1980) Significance of authigenic quartz euhedra after sulfates: example from the lockport formation (middle silurian) of New-York. J Sediment Petrol 50:1299–1304

Glunk C, Dupraz C, Braissant O, Gallagher KL, Verrecchia EP, Visscher PT (2011) Microbially mediated carbonate precipitation in a hypersaline lake, big pond (eleuthera, bahamas). Sedimentology 58:720–736

Grimes ST, Brock F, Rickard D, Davies KL, Edwards D, Briggs DEG, Ronald JP (2001) Understanding fossilization: experimental pyritization of plants. Geology 29:123

Heindel K, Birgel D, Brunner B, Thiel V, Westphal H, Gischler E et al (2012) Post-glacial microbialite formation in coral reefs of the Pacific, Atlantic, and Indian Oceans. Chem Geol 304–305(39):117–130

Heindel K, Richoz S, Birgel D, Brandner R, Klügel A, Krystyn L, Baud A, Horack M, Mobtat T, Pekmana J (2015) Biogeochemical formation of calyx-shaped carbonate crystal fans in the subsurface of the Early Triassic seafloor. Gondwana Res 27:840–861

Hips K, Haas J (2006) Calcimicrobial stromatolites at the Permian–Triassic boundary in a western Tethyan section, Bükk Mountains, Hungary. Sediment Geol 185:239–253

Huang SJ, Huang KK, Lü J, Lan YF (2012) Carbon isotopic composition of Early Triassic marine carbonates, Eastern Sichuan Basin, China. Sci China Earth Sci 55(12):2026–2038. doi:10.1007/s11430-012-4440-1

Ji W, Tong J, Zhao L, Zhou S, Chen J (2011) Lower–middle triassic conodont biostratigraphy of the Qingyan section, Guizhou province, Southwest China. Palaeogeogr Palaeoclimatol Palaeoecol 308:213–223

Joachimski MM, Lai X, Shen S, Jiang H, Luo G, Chen B, Sun YD (2012) Climate warming in the latest permian and the permian–triassic mass extinction. Geology 40:195–198

Joye SB, Bowles MW, Samarkin VA, Hunter KS, Niemann H (2010) Biogeochemical signatures and microbial activity of different cold-seep habitats along the Gulf of Mexico deep slope. Deep Sea Res Part II 57:1990–2001

Kah C, Riding R (2007) Mesoproterozoic carbon dioxide levels inferred from calcified cyanobacteria. Geology 35:799–802

Kaźmierczak J, Altermann W (2002) Neoarchean biomineralization by benthic cyanobacteria. Science 298:2351

Kaźmierczak J, Kempe S, Kremer B, López-García P, Moreira D, Tavera R (2011) Hydrochemistry and microbialites of the alkaline crater lake Alchichica, Mexico. Facies 57:543–570

Kershaw S, Li Y, Crasquin-Soleau S, Feng QL, Mu XN, Collin PY, Reynolds A (2007) Earliest Triassic microbialites in the South China Block and other areas; controls on their growth and distribution. Facies 53(3):409–425

Kershaw S, Crasquin S, Collin PY, Li Y, Feng Q, Forel MB (2009) Microbialites as disaster forms in anachronistic facies following the end-permian mass extinction: a discussion. Aust J Earth Sci 56:809–813

Kershaw S, Crasquin S, Forel MB, Randon C, Collin PY, Kosun E, Richoz B, Baud A (2011) Earliest triassic microbialites in Çürük dag, southern turkey; composition, cyclicity and controls on formation. Sedimentology 58:739–755

Kershaw S, Crasquin S, Li Y, Collin PY, Forel MB, Mu XN, Baud A, Wan Y, Xie SC, Maurer F, Li G (2012) Microbialites and global environmental change across the Permian–Triassic boundary: a synthesis. Geobiology 10:25–47

Kolber ZS, Plumley FG, Lang AS, Beatty JT, Blankenship RE, Vandover CL (2001) Contribution of aerobic photoheterotrophic bacteria to the carbon cycle in the ocean. Science 292:2492–2495

Lindenthal A, Langmann B, Paetsch J, Lorkowski I, Hort M (2012) The ocean response to volcanic iron fertilisation after the eruption of kasatochi volcano: a regional scale biogeochemical ocean model study. Biogeosciences Discuss 10:3715–3729

Liu ZL (1982) Fossil algae community from Wumishan formation in Jixian County of Hebei province. Acta Bot Sin 24:191–193 **(in Chinese)**

Liu XX, Liu ZL (1984) A study of late Precambrian microfoss algal community from Sui ning county, Jiang su province. Acta Micropalaeontol Sin 1:171–181 **(in Chinese)**

Luo M, Chen ZQ, Zhao L, Kershaw S, Huang J, Wu LL, Yang H, Fang YH, Huang YG, Zhang QY, Hu SX, Zhou CY, Wen W, Jia ZH (2014) Early middle triassic stromatolites from the luoping area, Yunnan province, Southwest China: geobiologic features and environmental implications. Palaeogeogr Palaeoclimatol Palaeoecol 412:124–140

Martin JPS (2010) The Girvanella-like remains from Messinian marine deposits (Sardinia, Italy): Lagerstätten paradigm for microbial biota? Annales de Paléontologie 96(2):33–50

Mastandrea A, Perri E, Russo F, Spadafora A, Tucker M (2006) Microbial primary dolomite from a norian carbonate platform: northern calabria, Southern Italy. Sedimentology 53:465–480

Mata SA, Bottjer DJ (2012) Microbes and mass extinctions: paleoenvironmental distribution of microbialites during times of biotic crisis. Geobiology 10:3–24

Noffke N, Awramik SM (2013) Stromatolites and miss—differences between relatives. Gsa Today 23:4–9

Ohfuji H, Rickard D (2005) Experimental syntheses of framboids-a review. Earth Sci Rev 71:147–170

Olgun N, Duggen S, Croot PL, Delmelle P, Dietze H, Schacht U, Garbe-Schönberg D (2011) Surface ocean iron fertilization: the role of airborne volcanic ash from subduction zone and hot spot volcanoes and related iron fluxes into the Pacific Ocean. Glob Biogeochem Cycles 25:1052–1054

Pacton M, Gorin G, Vasconcelos C, Gautschi HP, Barbarand J (2010) Structural arrangement of sedimentary organic matter: nanometer-scale spheroids as evidence of a microbial signature in early diagenetic processes. J Sediment Res 80:919–932

Payne JL, Lehrmann DJ, Jiayong W, Orchard MJ, Schrag DP, Knoll AH (2004) Large perturbations of the carbon cycle during recovery from the end-permian extinction. Science 305:506–509

Peckmann J, Thiel V (2004) Carbon cycling at ancient methane–seeps. Chem Geol 205:443–467

Perri E, Spadafora A (2011) Evidence of microbial biomineralization in modern and ancient stromatolites. Cell Origin Life Extrem Habitat Astrobiol 18:631–649

Perri E, Tucker ME (2007) Bacterial fossils and microbial dolomite in triassic stromatolites. Geology 35:207–210

Perri E, Tucker ME, Spadafora A (2012) Carbonate organo-mineral micro- and ultrastructures in sub-fossil stromatolites: Marion Lake, South Australia. Geobiology 10:105–117

Pfennig N (1968) Chlorobium phaeobacteroides nov. spec. und c. phaeovibrioides nov. spec. zwei neue arten der grünen schwefelbakterien. Archiv Für Mikrobiol 63:224–226

Pfennig N (1977) Phototrophic green and purple bacteria: a comparative, systematic survey. Annu Rev Microbiol 31:275–290

Pfennig N (1978) *Rhodocyclus purpureus* gen. nov. and sp. nov., a ring-shaped, vitamin B12-requiring member of the family rhodospirillaceae. Soc Gen Microbiol 2:283–288

Pruss SB, Bottjer DJ, Corsetti FA, Baud A (2006) A global marine sedimentary response to the end-permian mass extinction: examples from southern Turkey and the western United States. Earth Sci Rev 78:193–206

Reid RP, Visscher PT, Decho AW, Stolz JF, Bebout BM, Dupraz C (2000) The role of microbes in accretion, lamination and early lithification of modern marine stromatolites. Nature 406:989–992. doi:10.1038/35023158

Reitner J, Neuweiler F (1995) Mud mounds: a polygenetic spectrum of fine-grained carbonate buildups. Facies 32:1–70

Richoz S, Baud A, Krystyn L, Twitchett R, Marcoux J (2005) Permo–Triassic deposits of the Oman Mountains: from basin and slope to the shallow platform. In: 24th IAS regional Meeting, Post-Conference Excursion A 13, pp 1–57

Rickard DT (1970) The origin of framboids. Lithos 3:269–293

Riding R (1991) Calcareous algae and stromatolites. Springer, Berlin, pp 55–87

Riding R (2000) Microbial carbonates: the geological record of calcified bacterial–algal mats and biofilms. Sedimentology 47:179–214

Riding R, Liang L (2005) Geobiology of microbial carbonates: metazoan and seawater saturation state influences on secular trends during the Phanerozoic. Palaeogeogr Palaeoclimatol Palaeoecol 219:105–115

Russo PF, Neri C, Mastandrea A, Baracca A (1997) The mud mound nature of the cassian platform margins of the dolomites a case history: the cipit boulders from punta grohmann (Sasso Piatto Massif, Northern Italy). Facies 36:25–36

Russo F, Mastandrea A, Stefani M, Neri C (2000) Carbonate facies dominated by syndepositional cements: a key component of Middle Triassic platforms. The Marmolada case history (Dolomites, Italy). Facies 42:211–226

Sano H, Nakashima K (1997) Lowermost Triassic (Griesbachian) microbial bindstone–cementstone facies southwest Japan. Facies 36:1–24

Schubert JK, Bottjer DJ (1992) Early triassic stromatolites as post-mass extinction disaster forms. Geology 20:883–884

Schubert JK, Bottjer DJ (1995) Aftermath of the Permian-Triassic mass extinction event: Paleoecology of Lower Triassic carbonates in the western USA. Palaeogeogr Palaeoclimatol Palaeoecol 116(1–2):1–39

Shapiro RS (2000) A comment on the systematic confusion of thrombolites. Palaios 15:166–169

Shi ZQ, Zeng DY, Xiong ZJ, Zhang H (2010) Sedimentary records of triassic megamonsoon in upper Yangtze area. Bull Mineral Petrol Geochem 29:164–172

Song HJ, Tong JN, Xiong YL, Sun DY, Tian L, Song HY (2012) The large increase of δ13C carb-depth gradient and the end-permian mass extinction. Sci China Earth Sci 55(7):1101–1109

Song HY, Tong JN, Algeo TJ, Song HJ, Qiu HO, Zhu YY, Bates S, Lyons TW, Luo GM, Kump LR (2014) Early triassic seawater sulfate drawdown. Geochim Cosmochim Acta 128:95–113

Spadafora A, Perri E, Mckenzie JA, Vasconcelos C (2010) Microbial biomineralization processes forming modern ca:mg carbonate stromatolites. Sedimentology 57:27–40

Sun YD, Joachimski MM, Wignall PB, Chunbo Y, Yanlong C, Haishui J, Wang L, Lai X (2012) Lethally hot temperatures during the early triassic greenhouse. Science 338:366–370

Tong JN, Qiu HO, Zhao LS, Zuo JX (2002) Lower Triassic inorganic carbon isotope excursion in Chaohu, Anhui Province, China. J China Univ Geosci 13:98–106

Tong JN, Zhao LS, Zuo JX, Hansen HJ (2005) An integrated Lower Triassic sequence in Chaohu, Anhui Province. Earth Sci J China Univ Geosci 30:53–61

Tong J, Zuo J, Chen ZQ (2007) Early Triassic carbon isotope excursions from South China: proxies for devastation and restoration of marine ecosystems following the end-Permian mass extinction. Geol J 42:371–389

Visscher PT, Stolz JF (2005) Microbial mats as bioreactors: populations, processes, and products. Palaeogeogr Palaeoclimatol Palaeoecol 219:87–100

Visscher PT, Reid RP, Bebout BM, Hoeft SE, Thompson MJA (1998) Formation of lithified micritic laminae in modern marine stromatolites (bahamas): the role of sulfur cycling. Am Mineral 83:1482–1493

Visscher PT, Reid RP, Bebout BM (2000) Microscale observations of sulfate reduction: correlation of microbial activity with lithified micritic laminae in modern marine stromatolites. Geology 28(10):919–922

Voorhies AA, Biddanda BA, Kendall ST, Jain S, Marcus DN, Nold SC, Dick GJ (2012) Cyanobacterial life at low O2: community genomics and function reveal metabolic versatility and extremely low diversity in a Great Lakes sinkhole mat. Geobiology 10:250–267

Wilkin RT, Barnes HL (1996) Pyrite formation by reactions of iron monosulfides with dissolved inorganic and organic sulfur species. Geochim Cosmochim Acta 60:4167–4179

Wilkin RT, Barnes HL (1997) Formation processes of framboidal pyrite. Geochim Cosmochim Acta 61:323–339

Woods AD, Bottjer DJ, Corsetti FA (2007) Calcium carbonate seafloor precipitates from the outer shelf to slope facies of the Lower Triassic (Smithian-Spathian) UnionWash Formation, California, USA: sedimentology and palaeobiological significance. Palaeogeogr Palaeoclimatol Palaeoecol 252:281–290

Wright DT, Wacey D (2005) Precipitation of dolomite using sulphate-reducing bacteria from the Coorong region, South Australia: significance and implications. Sedimentology 52:987–1008

Wu FM (1985) New material of bivalves from the early triassic in Fujian. Acta palaeontol sin 24:395–402 **(in Chinese)**

Xie SC, Pancost RD, Yin HF, Wang HM, Evershed RP (2005) Two episodes of microbial change coupled with permo/triassic faunal mass extinction. Nature 434:494–497

Yan CB, Wang L, Jiang HJ, Wignall PB, Sun YD, Chen YL, Lai XL (2013) Uppermost permian to Lower Triassic conodonts at Bianyang section, Guihzou province, South China. Palaios 28:509–522

Yang SR, Wang XP, Hao WC (1986) Early Triassic bivalve assemblage of western Guingxi. J Stratigr 10:88–97

Yang H, Chen ZQ, Wang Y, Tong J, Song H, Chen J (2011) Composition and structure of microbialite ecosystems following the end-Permian mass extinction in South China. Palaeogeogr Palaeoclimatol Palaeoecol 308:111–128

Yin HF, Huang SJ, Zhang KX (1992) The effects of volcanism on the Permian-Triassic mass extinction in South China. In: Sweet WC, Yang ZY, Dickins JM, Yin HF (eds) Permo-Triassic Events in the Eastern Tethys. Cambridge University Press, London, pp 146–157